



TECHNICAL ARTICLE

Effect of Al Content on Formation Mechanism of AlN and MnS Inclusions in Fe-5Mn-xAl-0.15C-0.23Si Medium Mn Steel

LI-BIN JIN,¹ SHU-GUO ZHENG,^{1,2} and MIAO-YONG ZHU¹

1.—School of Metallurgy, Northeastern University, 3-11, Wenhua Road, Shenyang 110819, China.
2.—e-mail: zhengsg@smm.neu.edu.cn

The effect of Al content on the formation mechanism of AlN and MnS inclusions in Fe-5Mn-xAl-0.15C-0.23Si ($x = 0.018\%$, 0.95% , 1.93% , 2.97%) medium Mn steel was investigated under as-cast conditions by microstructure observation, thermodynamic analyses, and the Clyne–Kurz microsegregation model. The effect of Al content on the partition coefficient, diffusion coefficient, and secondary dendrite arm spacing was explored first, and then these parameters under different Al contents were used in the Clyne–Kurz model to predict the solute concentration in the residual liquid steel. The results showed that, with increasing Al content, the solute partition coefficients were easily influenced, and the order of the influence was $S > C > N > Al > Mn$. Among these, the average partition coefficients of S showed a large downward trend (from 0.0107 to 0.0060), while Mn showed little change (approximately 0.71). Based on an electron probe microanalyzer, the partition coefficients of the solutes S, C, N, and Mn were all lower than 1, while solute Al was higher than 1, which were consistent of the results by Thermo-Calc calculations. With the Al content increasing from 0.95% to 2.97%, the precipitation temperature of AlN increased from 1730 K to 1759 K. The local growth time of MnS increased from 0.80 s to 4.96 s.

INTRODUCTION

Recently, with the increasing demand for achieving energy savings and emission reduction in the automotive industry, automotive steel has been set high requirements. Medium Mn steel has received much attention owing to high strength, high ductility, and excellent tensile strain-hardening performance.^{1,2} Aluminum is a lightweight element commonly used in medium Mn steel.^{3,4} The addition of Al not only reduces weight but also improves elongation by increasing the ferrite content.⁵ Accordingly, the Fe-Mn-Al-C system is gradually replacing the Fe-Mn-C system because of its advantages, and occupies a large market share in automotive steel.^{6,7} However, adding high Al into medium Mn steel may result in a large amount of AlN and MnS forming directly in the liquid steel or precipitate in the residual liquid steel during the

subsequent solidification process, which limits the combination of high strength and ductility.^{8,9} Thus, it is necessary to investigate the formation mechanism of AlN and MnS inclusions.

Many assumed microsegregation models have been presented to predict the solute concentration in residual liquid steel during the solidification process, such as the lever-rule model,¹⁰ the Scheil model,¹¹ the Brody–Flemings model,¹² the Clyne–Kurz model,¹³ the Ohnaka model,¹⁴ and the Voller–Beckermann model.¹⁵ However, the applicability of some parameters in those models has usually been neglected, such as the solute partition coefficient. In fact, it is an important parameter which determines the redistribution trend of solute elements between the liquid phase and the solid phase, and is easily influenced by the phase composition. Al, as a ferrite-forming element, can stabilize the δ phase during steel solidification, and, therefore, the addition of Al into medium Mn steel has some influence on the phase composition. The adding of Al into medium Mn steel will change the solubility of solute elements between the liquid phase and the solid (δ and

(Received October 3, 2023; accepted April 25, 2024;
published online May 28, 2024)

γ) phase, inducing the variation of solute partition coefficients during solidification. Under different Al contents, the variation of the partition coefficient should be considered in microsegregation models, which may accurately describe the solute microsegregation behavior to further account for the formation of AlN and MnS inclusions. Among the microsegregation models, the Clyne–Kurz model is widely applicable considering the finite non-zero diffusion of solute elements in the solid phase, and can accurately predict the solute concentration in residual liquid steel during the solidification process.^{16–18} Currently, in the research of the formation mechanism of AlN and MnS inclusions in Fe-Mn-Al-C steel, the partition coefficients of solutes Al, N, Mn, and S were simplified to the same value in Fe-Mn-Al-C steel with various Mn contents.^{19–21} Alba et al.²⁰ analyzed the formation of AlN in Fe-xMn-3Al-0.12C ($x = 2\%, 5\%, 20\%$) steel by the lever-rule model and the Scheil model. However, the variation of the partition coefficients of Al and N under different Mn contents were neglected in their study. With the increase of the Mn content, the values of the partition coefficients of Al and N were invariant, and were still 0.6 and 0.27, respectively. They found that the AlN will precipitate first with the increase of Mn content. When the Mn contents were 2% and 5%, the solid fractions (f_s) of AlN precipitation were 0.574 and 0.422, respectively. With Mn content further increasing to 20%, the AlN can form in the liquid steel. Moreover, Liu et al.²¹ reported the formation of MnS in Fe-xMn-7Al-0.7C ($x = 3\%, 10\%, 20\%, 30\%$) steel by the Voller–Beckermann model, but the solute partition coefficients of Mn and S were also unchanged under different Mn contents. With increasing of Mn content, the f_s of MnS precipitation decreased from 0.91 to 0.43. As mentioned above, all these values of partition coefficients for solutes Al, N, Mn, and S were invariant, which led to insufficient accuracy of the predictions of the solute concentration in the residual liquid steel. Obviously, the Al content has an effect on the solute partition coefficients and also the formation of AlN and MnS. However, studies on the formation mechanism of AlN and MnS inclusions in medium Mn steels with various Al contents have rarely been reported. In this study, the effect of Al content on the partition coefficient, diffusion coefficient, and secondary dendrite arm spacing in medium Mn steel have been explored, and then these parameters under different Al contents have been used in the Clyne–Kurz model to predict the solute concentration. The Fe-5Mn-(0, 1, 2, 3)Al-0.15C-0.23Si medium Mn steels were prepared, using a 50-kg vacuum-induction furnace. The formation mechanisms of AlN and MnS under the as-cast conditions were analyzed by thermodynamic calculations and the Clyne–Kurz model. Furthermore, an electron probe microanalyzer (EPMA) was

employed for dendrite structure observation and chemical composition analysis to describe the microsegregation behavior of the solute elements.

EXPERIMENTAL PROCEDURES AND THERMODYNAMIC CALCULATIONS

Material Preparation

The medium Mn steels with various Al contents were smelted using a 50-kg intermediate frequency induction furnace, and the compositions of these steels are listed in Table I. The initial average N (0.0029%) and S (0.0062%) contents have been compared with the critical N and S contents of AlN and MnS for the stability diagram (Fig. 2), which appears in the subsequent discussion. The dimensions of the steel ingot and the positions of the specimen are shown in Fig. 1.

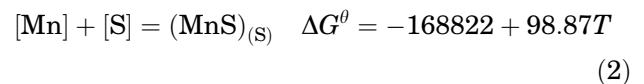
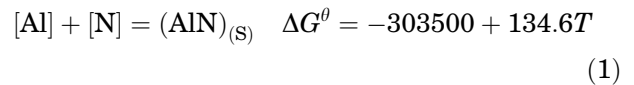
Microstructure Characterization

The specimens used for observation were mechanically ground and polished, and then they were etched in 5% saturated picric acid solution, and the dendritic structure was observed using a digital microscope (AxioCam MRC5). The secondary dendrite arm spacing was analyzed by the Image-Pro Plus 6.0 image software, and the dendrite structure and chemical composition were characterized using EPMA (JXA-8530F).

Thermodynamic Calculations

Thermodynamic Equations of AlN and MnS Formation in Liquid Steel

The reaction equations of AlN and MnS formation in liquid steel are:^{22,23}



Then, the solubility constants of AlN and MnS were calculated by:

$$\begin{aligned} \log K_{\text{AlN}} &= -\log(f_{\text{Al}}) \cdot [\% \text{ Al}] - \log(f_{\text{N}}) \cdot [\% \text{ N}] \\ &= \frac{-15850}{T} + 7.03 \end{aligned} \quad (3)$$

$$\begin{aligned} \log K_{\text{MnS}} &= -\log(f_{\text{Mn}}) \cdot [\% \text{ Mn}] - \log(f_{\text{S}}) \cdot [\% \text{ S}] \\ &= \frac{-8817}{T} + 5.16 \end{aligned} \quad (4)$$

where f_i is the activity coefficient of component I relative to the dilute solution. The values of f_i were calculated by:

Table I. Chemical compositions of medium Mn steels (wt.%)

Specimens	C	Mn	Al	Si	Nb	V	N	S	P	O
0 Al	0.15	5.05	0.018	0.23	0.06	0.05	0.0029	0.0060	0.0050	0.0015
1 Al	0.15	4.98	0.95	0.23	0.05	0.05	0.0032	0.0063	0.0050	< 0.0005
2 Al	0.17	4.96	1.93	0.23	0.07	0.04	0.0025	0.0059	0.0040	< 0.0005
3 Al	0.15	5.04	2.97	0.23	0.06	0.04	0.0030	0.0066	0.0040	< 0.0005
Average	–	–	–	–	–	–	0.0029	0.0062	–	–

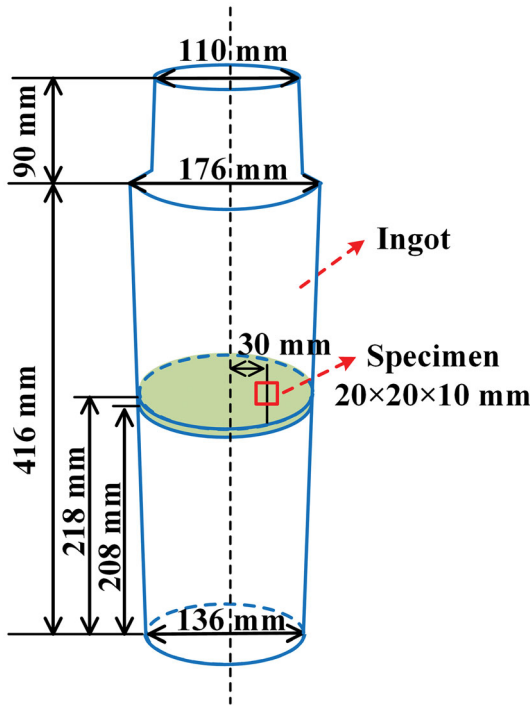


Fig. 1. The dimensions of the steel ingot and the positions of the specimen.

$$\log f_i = \sum (e_i^j \cdot [\text{pct } j] + r_i^j \cdot [\text{pct } j]^2) \quad (5)$$

where $i = \text{Al, N, Mn, S}; j = \text{C, Al, N, Mn, S, Si, P, O}$.

The first-order interaction parameters (e_i^j) and the second-order interaction parameters (r_i^j) are from our previous study.¹⁸ Accordingly, the equilibrium solubility product of AlN formation can be derived from Eqs. 1, 3, and 5:

$$K_{\text{AlN}} = [\text{pct Al}][\text{pct N}] = \begin{cases} 10^{7.104-15850/T} & \text{Al} = 0.95 \\ 10^{7.089-15850/T} & \text{Al} = 1.93 \\ 10^{7.083-15850/T} & \text{Al} = 2.97 \end{cases} \quad (6)$$

When the Al content was 0.018%, the AlN cannot precipitate in the liquid steel or the residual liquid steel during subsequent solidification process due to the lower Al content. Therefore, for the 0.018% Al steel, the formation of AlN is not discussed in this study.

Similarly, the MnS formation in liquid steel were calculated by Eqs. 2, 4, and 5:

$$K_{\text{MnS}} = [\text{pct Mn}][\text{pct S}] = \begin{cases} 10^{5.276-8817/T} & \text{Al} = 0.018 \\ 10^{5.236-8817/T} & \text{Al} = 0.95 \\ 10^{5.192-8817/T} & \text{Al} = 1.93 \\ 10^{5.152-8817/T} & \text{Al} = 2.97 \end{cases} \quad (7)$$

When the actual product of [% Al] and [% N], [% Mn], and [% S] reached the values of K_{AlN} and K_{MnS} at the liquidus temperature, AlN and MnS, respectively, formed in the liquid steel. With the increasing Al content, the values of K_{AlN} and K_{MnS} decreased, which led to the possibility of the formation of AlN and MnS gradually increasing in the liquid steel.

Microsegregation Models of AlN and MnS Formation During the Solidification Process

The microsegregation of solute elements increased the actual concentration product in the residual liquid phase, and AlN and MnS may be forming during the solidification process. Accordingly, many assumed microsegregation models have been proposed to account for the redistribution of solute elements.

The lever-rule model¹⁰ assumes the solute elements completely diffuse between the liquid and solid phase:

$$C_L = C_0/[1 - (1 - k_i)f_s] \quad (8)$$

However, the Scheil model¹¹ neglects the diffusion of solute elements in the solid phase:

$$C_L = C_0[1 - f_s]^{(k_i-1)} \quad (9)$$

However, the idealized microsegregation models of the lever-rule and the Scheil were not reasonable enough. The lever-rule model thinks that the diffusion rate of any solute element is infinite in the solid phase. The Scheil model considers that the diffusion rate of any solute element is zero in the solid phase. During solidification, the diffusion rate of any solute element will not be zero or infinity in the solid phase. Accordingly, the finite non-zero diffusion of solute elements in the solid phase should be considered to predict the solute concentration during solidification. The Brody–Flemings model¹² assumes finite non-zero diffusion of solute elements

in the solid phase, and the results are more suitable for the actual solidification process:

$$C_L = C_0 [1 - (1 - \beta_i k_i) f_s]^{(k_i - 1) / (1 - \beta_i k_i)} \quad (10)$$

where β_i is the back-diffusion parameter, which is described as:

$$\beta_i = 2\alpha_i \quad (11)$$

where α_i is the Fourier number of solute i , as:

$$\alpha_i = \frac{4D_s t_f}{\lambda_s^2} \quad (12)$$

where t_f (s) is the local solidification time, defined as:

$$t_f = \frac{T_L - T_S}{C_R} \quad (13)$$

The Clyne–Kurz model¹³ modified the back-diffusion parameter (β_i) and ensured the reasonability in the physical, and is defined as:

$$\beta_i = 2\alpha [1 - \exp(-\frac{1}{\alpha})] - \frac{1}{2} \exp(-\frac{1}{2\alpha}) \quad (14)$$

It is obvious that the lever-rule model and the Scheil model were not accurate enough. The Brody–Flemings improved their accuracy due to the finite non-zero diffusion of solute elements being considered in the solid phase. Based on the Brody–Flemings model, the Clyne–Kurz modified the back-diffusion parameter, which made the results more suitable for the actual solidification process. As mentioned above, when the four models appeared in the study, the Clyne–Kurz model could be directly used to calculate. Thus, in this study, we directly selected the Clyne–Kurz model to calculate the solute concentration in the residual liquid phase during solidification, as it was more accurate and widely applicable.^{16–18,24–26} In this study, the actual product concentrations of AlN and MnS during solidification of medium Mn (~ 5 Mn%) steel with various Al contents were calculated by the Clyne–Kurz model:

$$\begin{aligned} Q_{\text{AlN}} &= [\% \text{ Al}] [\% \text{ N}] \\ &= [\% \text{ Al}]_0 [(1 - (1 - \beta_{\text{Al}} k_{\text{Al}}) f_s)^{\frac{(k_{\text{Al}} - 1)}{(1 - \beta_{\text{Al}} k_{\text{Al}})}} [\% \text{ N}]_0 \\ &\quad [(1 - (1 - \beta_{\text{N}} k_{\text{N}}) f_s)^{\frac{(k_{\text{N}} - 1)}{(1 - \beta_{\text{N}} k_{\text{N}})}}] \end{aligned} \quad (15)$$

$$\begin{aligned} Q_{\text{MnS}} &= [\% \text{ Mn}] [\% \text{ S}] \\ &= [\% \text{ Mn}]_0 [(1 - (1 - \beta_{\text{Mn}} k_{\text{Mn}}) f_s)^{\frac{(k_{\text{Mn}} - 1)}{(1 - \beta_{\text{Mn}} k_{\text{Mn}})}} [\% \text{ S}]_0 \\ &\quad [(1 - (1 - \beta_{\text{S}} k_{\text{S}}) f_s)^{\frac{(k_{\text{S}} - 1)}{(1 - \beta_{\text{S}} k_{\text{S}})}}] \end{aligned} \quad (16)$$

where $[\% \text{ Al}]_0$, $[\% \text{ N}]_0$, $[\% \text{ Mn}]_0$ and $[\% \text{ S}]_0$ are the initial contents of Al, N, Mn, and S in the liquid steel, respectively and k_{Al} , k_{N} , k_{Mn} , and k_{S} are the equilibrium partition coefficients of Al, N, Mn, and S, respectively.

When the actual products, Q_{AlN} and Q_{MnS} , exceed the values of K_{AlN} and K_{MnS} , calculated by Eqs. 6 and 7, respectively, AlN and MnS are able to form during the solidification process.

RESULTS AND DISCUSSION

Thermodynamics Analysis of AlN and MnS Formation in Liquid Steel

The stability diagram of AlN and MnS formation is shown in Fig. 2. The dashed and solid lines illustrate the solubility product of AlN and MnS at the liquidus (T_L) and solidus temperatures (T_S), respectively. It can be seen in Fig. 2a, with Al content increasing from 0.95% to 2.97%, that the N contents of the formation of AlN decreased from 0.0151% to 0.0049% at the liquidus temperature. However, the critical N contents of the formation of AlN inclusions were still higher than the initial average content of N (0.0029%), so AlN was unable to form in the liquid steel. As shown in Fig. 2b, with the Al content increasing from 0.018% to 2.97%, the S contents of the formation of MnS also decreased at the liquidus temperature, from 0.3960% to 0.3120%, which are much larger than the initial average content of S (0.0062%); therefore the MnS cannot precipitate in the liquid steel.

Variable Parameters During the Solidification Process

As seen in Fig. 2, the AlN and MnS were unable to form in the liquid steel. However, when the temperature was lower than the liquid temperature, the microsegregation of solute elements will increase the actual concentration product in the residual liquid steel, and the AlN and MnS may be forming during solidification. The Clyne–Kurz model can be expressed as a function of the microsegregation of element i . These parameters contain the equilibrium partition coefficient (k_i) and diffusion coefficient (D^S), secondary dendrite arm spacing (λ_s), and cooling rate (C_R), which have been discussed to illustrate the variation. These parameters under different Al contents have been used in the Clyne–Kurz model.

The pseudo-binary phase diagram of Fe-5Mn-xAl-0.15C-0.23Si steel is shown in Fig. 3. It can be seen that the Al content influences and determines the phase transition during the steel solidification. The Al contents are 0.018, 0.95, 1.93, and 2.97% in the steel, which classified three solidification modes. Among them, when the Al content is 0.018%, it belongs to hyper-peritectic steel, and to the L + δ , L + δ + γ , and L + γ phases in turn, and the L + γ phase exists mainly during solidification. When the

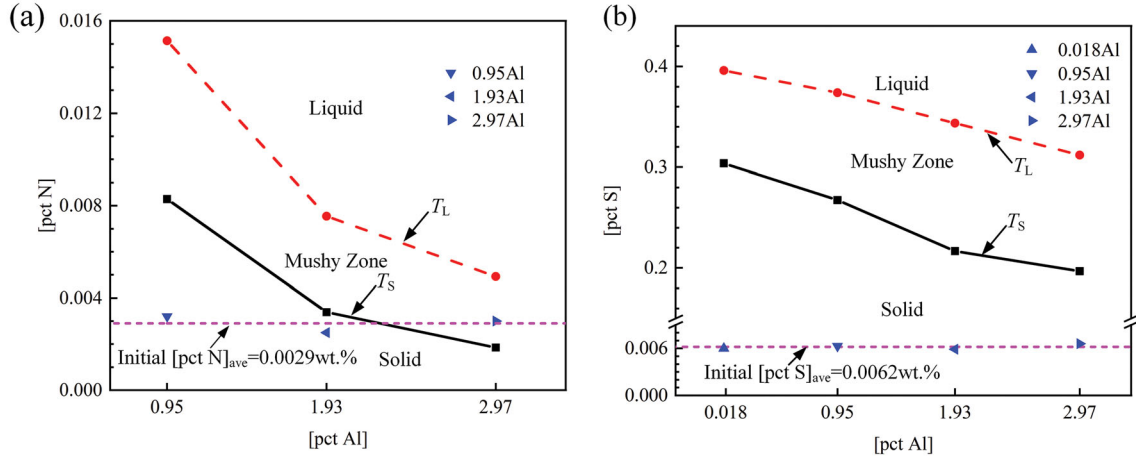


Fig. 2. The stability diagram of AIN and MnS formation: (a) AIN; (b) MnS.

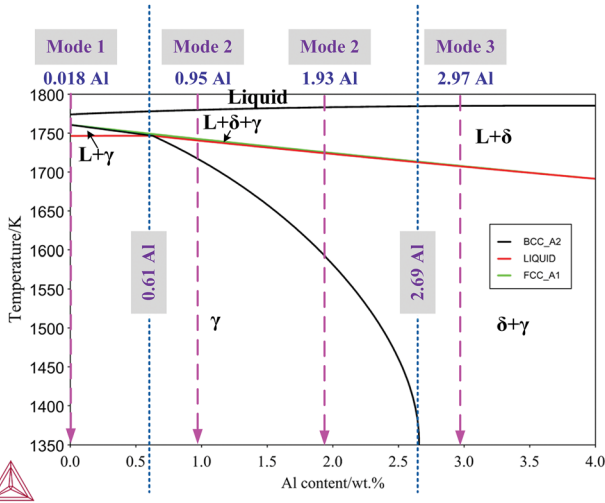


Fig. 3. The pseudo-binary phase diagram of Fe-5Mn-xAl-0.15C-0.23Si steel.

Al content is 0.61%, it is a critical Al content of the peritectic point of the steel. The steel belongs to hyper-peritectic steel when the Al content is lower than 0.61%. When the Al contents are 0.95 and 1.93%, they are hypo-peritectic steels, and the L + δ , L + δ + γ , and δ + γ phases in turn. When the Al content is higher than 2.69%, the range of the single γ phase cannot exist due to the large content of the δ phase after the peritectic reaction (L + δ \rightarrow γ) finishes. Although the 2.97% Al steel also belongs to hypo-peritectic steel, the steel is classified as another mode. The solidification mode of Fe-5Mn-xAl-0.15C-0.23Si steel concludes as follows:

- Mode 1: 0.018% Al: L \rightarrow L + δ \rightarrow L + δ + γ \rightarrow L + γ \rightarrow γ
 Mode 2: 0.95 and 1.93% Al: L \rightarrow L + δ \rightarrow L + δ + γ \rightarrow δ + γ \rightarrow γ
 Mode 3: 2.97% Al: L \rightarrow L + δ \rightarrow L + δ + γ \rightarrow δ + γ

As seen in Table II, with the increase of Al content, the solidification starting temperature (liquids temperature) increased while the ending temperature (solidus temperature) decreased, and the temperature range of the solidification process increased from 40.1 K to 88.3 K. The temperature range of the L + δ phase coexisting zone gradually increased, from 14.5 K to 87.0 K, and the proportion of the L + δ in the whole solidification temperature range ($\frac{\Delta T_{L+\delta}}{T_L - T_S}$), increased from 36.2% to 98.5%. Therefore, under different Al contents, the solidification modes of Fe-5Mn-xAl-0.15C-0.23Si steel were quite different, which caused a significant effect on these parameters of the Clyne-Kurz model.

Figure 4 shows the equilibrium partition coefficients during Fe-5Mn-xAl-0.15C-0.23Si steel solidification. In the δ /L phase, the Al content has a slight influence on the partition coefficients of solutes Mn and C, while it has a great effect on solutes S, N, and Al. In the δ + γ /L phase, the solute partition coefficients contain the δ /L and γ /L phases, which were different because of the difference in solubility. $k^{\delta+\gamma/L}$ was calculated by:^{27,28}

$$k^{\delta+\gamma/L} = m_\delta \cdot k^{\delta/L} + m_\gamma \cdot k^{\gamma/L} \quad (17)$$

$$m_\delta + m_\gamma = 1 \quad (18)$$

where $k^{\delta/L}$, $k^{\gamma/L}$, and $k^{\delta+\gamma/L}$ are the solute partition coefficients in the δ /L, γ /L, and δ + γ /L interfaces, respectively, and m_δ and m_γ are the mass fractions of δ and γ in the solid phase, respectively. In the γ /L phase, the Al content has little effect on solutes Mn, C, and Al, while it has a great influence on S and N.

The average values of the partition coefficients of the solute elements are shown in Fig. 4f. With increasing Al content, k_{Mn}^{ave} shows little change and is approximately 0.71, k_N^{ave} first decreased from 0.47 to 0.30 (0.018–0.95%) and then presented a

Table II. The solidification temperature range and phase transition temperature

Al	L + δ range (K)			L + δ + γ range (K)			L + γ range (K)			$T_L - T_S$
	$T_{start}^{L+\delta}$	$T_{end}^{L+\delta}$	$\Delta T_{L+\delta}$	$T_{start}^{L+\delta+\gamma}$	$T_{end}^{L+\delta+\gamma}$	$\Delta T_{L+\delta+\gamma}$	$T_{start}^{L+\gamma}$	$T_{end}^{L+\gamma}$	$\Delta T_{L+\gamma}$	
0.018	1770.1	1755.6	14.5	1755.6	1754.7	0.9	1754.7	1730.0	24.7	40.1
0.95	1776.1	1733.2	42.9	1733.2	1725.5	7.7	-	-	-	50.6
1.93	1778.2	1714.6	63.6	1714.6	1708.8	5.8	-	-	-	69.4
2.97	1780.9	1693.9	87.0	1693.9	1692.6	1.3	-	-	-	88.3

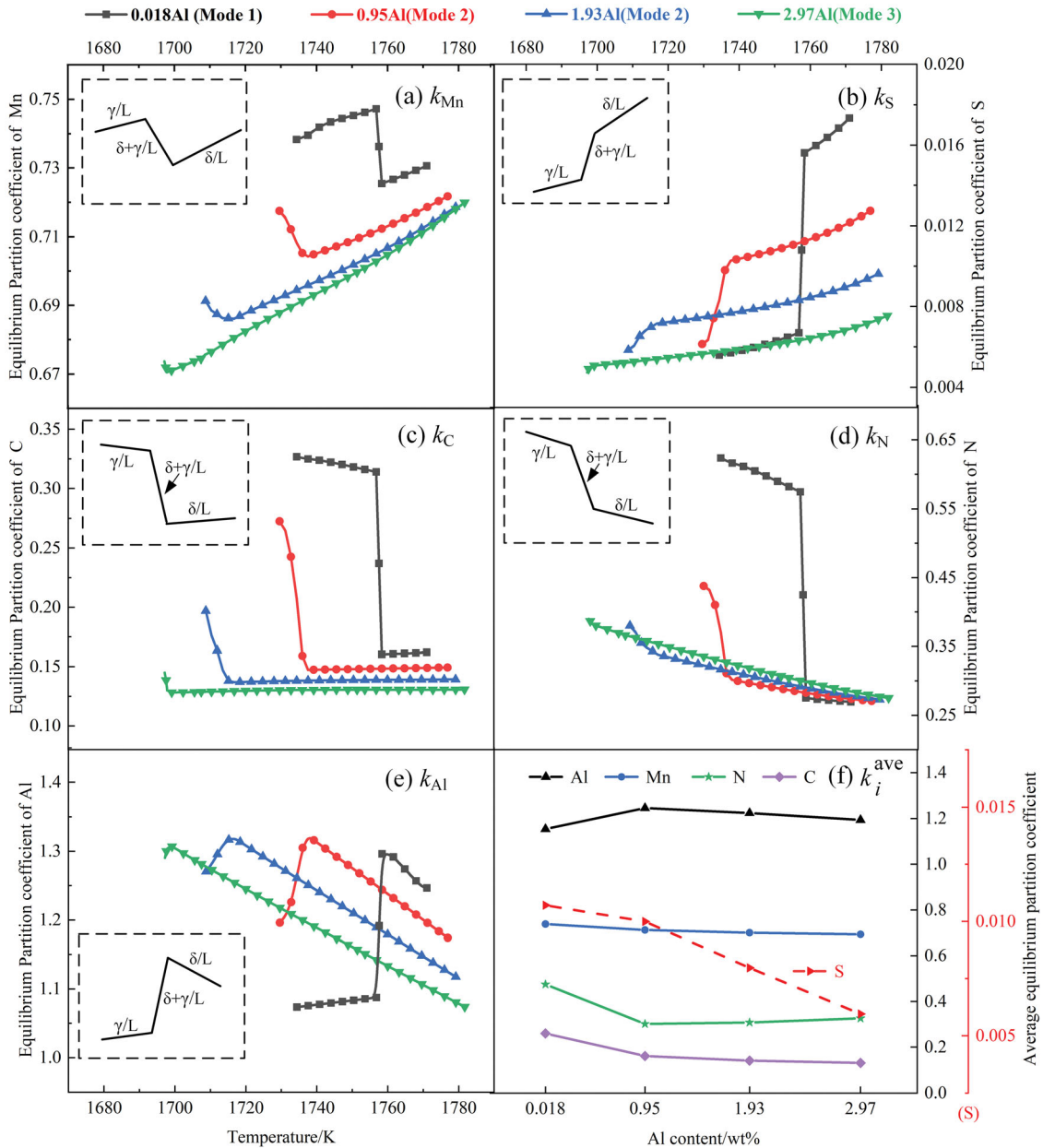


Fig. 4. The equilibrium partition coefficients of solute elements calculated by Thermo-Calc software: (a) k_{Mn} ; (b) k_S ; (c) k_C ; (d) k_N ; (e) k_{Al} ; (f) k_i^{ave} .

slight increase to 0.33 (2.97% Al), and $k_{\text{Al}}^{\text{ave}}$ showed the reverse trend with N, first increasing from 1.15 to 1.25, and then decreasing to 1.19 (2.97%). The values of the solute partition coefficients were further away from 1, illustrating that the segregation degree of the solute elements is becoming more serious. Although the partition coefficients of solutes Al and N had the reverse variable trend with the increase of Al content, the variation of segregation degree was nearly consistent. As seen in Fig. 4d, the solute N easily enriched in the γ phase compared with the δ phase ($k_{\text{N}}^{\gamma/\text{L}} > k_{\text{N}}^{\delta/\text{L}}$), and the γ/L coexisting zone only exists in the 0.018% Al steel, and, therefore, the value of $k_{\text{N}}^{\text{ave}}$ was the largest (0.018%). Furthermore, with the Al content increasing from 0.95% to 2.97%, the proportion of the δ/L coexisting zone gradually increased in the whole solidification process, and the $k_{\text{N}}^{\delta/\text{L}}$ was higher in 2.97% Al steel, and, therefore, the $k_{\text{N}}^{\text{ave}}$ presented a slight increase. Similarly, the $k_{\text{Al}}^{\text{ave}}$ was the smallest in the 0.018% Al steel, and, then, with the Al content increasing from 0.95% to 2.97%, the $k_{\text{Al}}^{\text{ave}}$ presented a slight decrease. The values of $k_{\text{S}}^{\text{ave}}$ and $k_{\text{C}}^{\text{ave}}$ decreased continuously with the increase of Al content. The solute S showed a large downward trend, from 0.0107 to 0.0060, and the values were much smaller than other solute elements.

In addition, the positive segregation or negative segregation of the solute elements did not change with increasing of the Al content. The partition coefficients of Mn, S, N, and C were all lower than 1 under different Al contents, which showed the positive segregation. Thus, those elements will segregate in the interdendritic area, enriching in the residual liquid steel during solidification. However, the solute Al was higher than 1, presenting the negative segregation, and, therefore, the Al will segregate in the dendrite, which will be enriched in the solid phase. In summary, the solute partition coefficients were easily influenced by the addition of Al during solidification, and the order of the influence was $\text{S} > \text{C} > \text{N} > \text{Al} > \text{Mn}$. Thus, under different Al contents, the variation of the solute partition coefficients should be considered, and then used in the Clyne–Kurz model.

The typical dendrite morphology of Fe-5Mn-xAl-0.15C-0.23Si steel is shown in Fig. 5. With the Al content increasing from 0.018% to 2.97% Al, the average secondary dendrite arm spacing (λ_{S}) changed little, and were $66 \pm 17 \mu\text{m}$, $68 \pm 20 \mu\text{m}$, $71 \pm 13 \mu\text{m}$, $67 \pm 19 \mu\text{m}$, respectively. The value

of λ_{S} can be used to predict the cooling rate, and investigators²⁹ have shown that the relationship was:

$$\lambda_{\text{S}} = 143.9 \cdot C_{\text{R}}^{-0.3616} \cdot C_{\text{C}}^{(0.5501-1.996C_{\text{C}})} \quad (19)$$

where C_{C} is the content of carbon (wt.%) and C_{R} is the cooling rate (K/s). Then, the cooling rate for the medium Mn steel ingots with various Al content during solidification was approximately 2.5 K/s. Therefore, the variation of the secondary dendrite arm spacing and cooling rate under different Al contents should be considered, and then used in the Clyne–Kurz model.

The results of EPMA have been widely used in Fe-Mn-Al-C steel to describe the microsegregation of solute elements in the solid phase and the residual liquid phase, or the dendrite and interdendritic areas.^{30–33} The EPMA composition maps of solute elements under different Al contents are shown in Fig. 6. The results show that the concentrations of solutes C, N, S, and Mn in the interdendritic area were higher than those in the dendrite under different Al contents, while the concentration distribution of solute Al was the opposite, which is consistent with the results of the Thermo-Calc calculations (Fig. 4). The concentrations of N and S were lower in the detecting matrix, because the initial contents of solutes S (0.0062%) and N (0.0029%) were lower than the other solute elements (C, Mn, and Al).

The distance of $1 \mu\text{m}$ shows a value in the process of determining the element content by the line scanning of EPMA. The calculated microsegregation ratio (= the element content in this position/the average element content in this line) of solutes C, N, S, Mn, and Al under different Al contents is shown in Fig. 7. Under different Al contents, the big difference of the microsegregation ratios of the solute elements existed in the interdendritic area and the dendrite. Among these, the larger microsegregation ratios appeared in the interdendritic area or dendrites, which depended on the positive segregation or negative segregation of the solutes. Solutes C, N, S, and Mn were positive segregation, enriching in the interdendritic area, and, therefore, their microsegregation ratios in the interdendritic area were higher than those in the dendrite. However, the solute Al was negative segregation, which enriched in the dendritic. Accordingly, its microsegregation ratio was larger in the dendritic. Under different Al contents, these microsegregation ratios of the solutes in the interdendritic area and dendrite all had good agreement with positive segregation or negative segregation of the solutes.

The standard deviation (SD) can describe the segregation degree for solute elements.³³ Based on the Fig. 7, the microsegregation ratios have been used to calculate the SD of those solute elements, and then the SDs are shown in Fig. 8. Under different Al contents, the SD of a solute element was

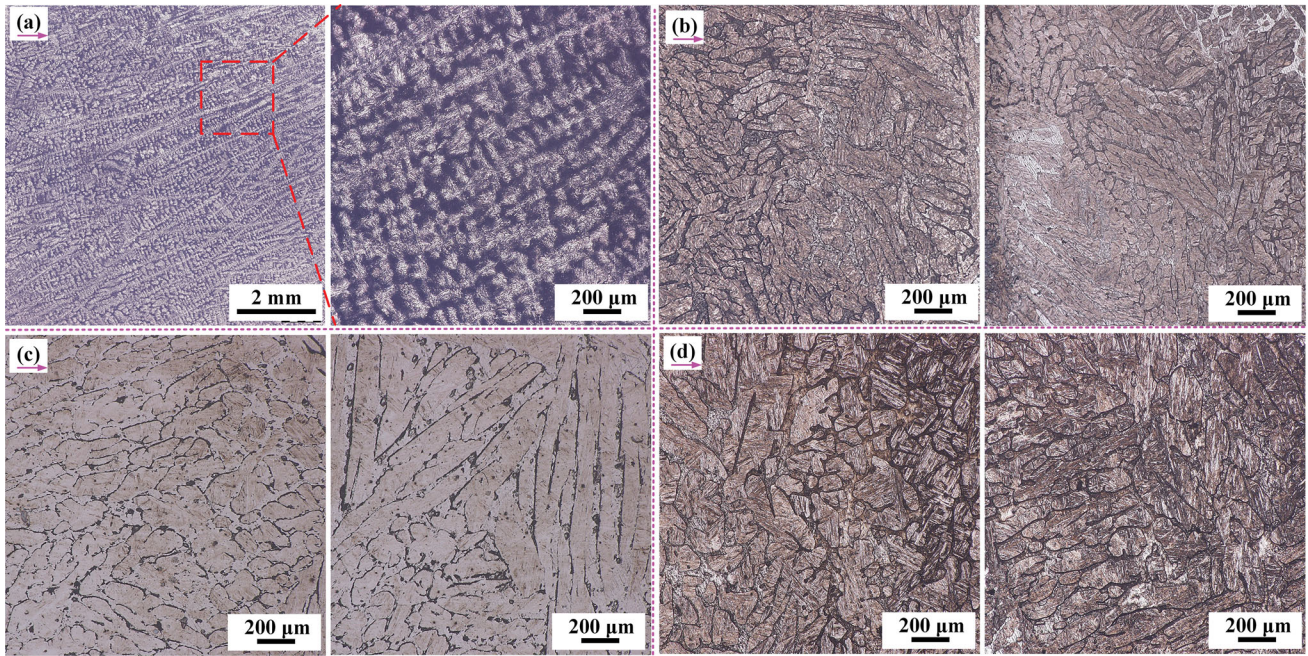


Fig. 5. Typical dendrite morphology: (a) 0.018 Al; (b) 0.95 Al; (c) 1.93 Al; (d) 2.97 Al.

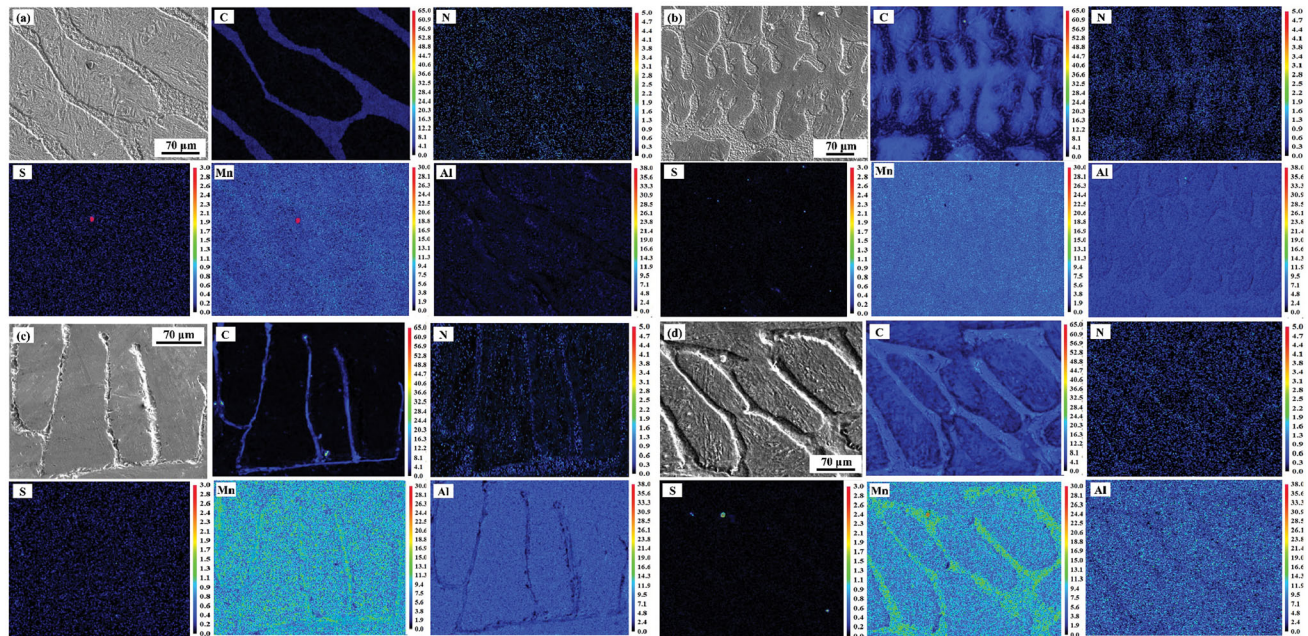


Fig. 6. EPMA composition maps of solute C, N, S, Mn, and Al: (a) 0.018 Al; (b) 0.95 Al; (c) 1.93 Al; (d) 2.97 Al.

greater and the segregation degree was more severe for this solute element. With the increase of Al content, the SD of solutes C, S, and Mn increased, which indicated their segregation degrees became severe. The SDs of solutes N and Al were the smallest when the Al content was 0.018%, presenting the smallest segregation degree, while the segregation degree of solutes N and Al was the most serious when the Al content was 0.95%, because the SD was the largest. Finally, the

segregation degree of solutes N and Al showed an alleviative trend on the whole with the Al content increasing from 0.95% to 2.97%.

Figure 9 shows the δ and γ phase fractions. With increasing Al content, the percentage of the δ phase increased while the γ phase decreased, while when the Al content was 0.018%, the solid phase was the single γ phase. The majority of the solid phase was the γ phase when the Al content was 0.95%. However, with the Al content increasing to 2.97%,

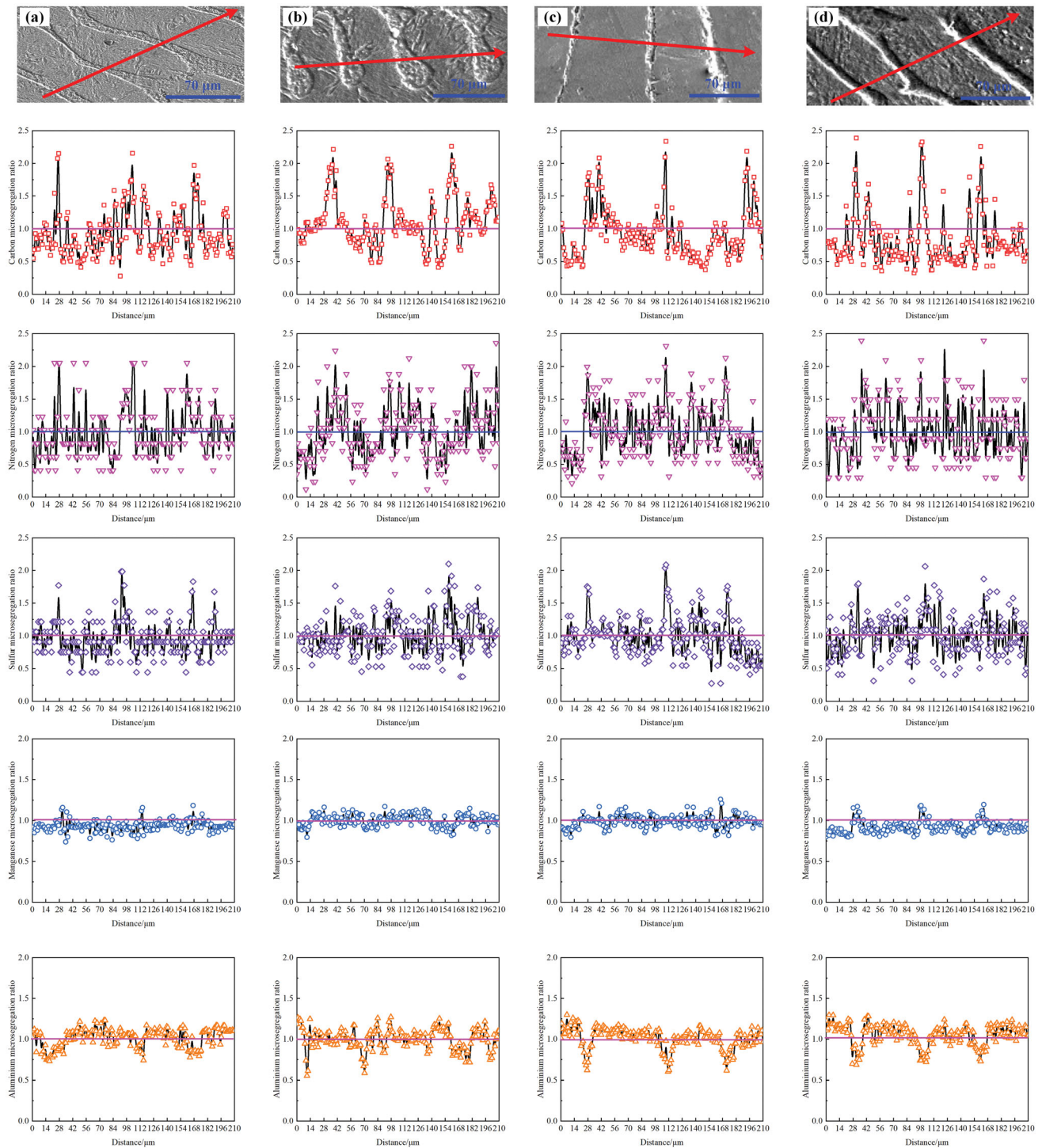


Fig. 7. EPMA composition line and microsegregation ratio of solute C, N, S, Mn and Al: (a) 0.018 Al; (b) 0.95 Al; (c) 1.93 Al; (d) 2.97 Al.

the solid phase was gradually occupied by the δ phase, and only a small amount of the γ phase formed at the later stage of solidification. The Al content had a great influence on the fractions of the δ and γ phases for Fe-5Mn-xAl-0.15C-0.23Si steel solidification, further changing the solubility of the solute elements between the liquid phase and the solid (δ and γ) phase.

Figure 10 shows the diffusion coefficients of solute elements in the solid phase during Fe-5Mn-xAl-0.15C-0.23Si steel solidification. In the δ phase, the Al content has a slight influence on the diffusion coefficients of solutes Mn, C, and S, while it has a great effect on solutes N and Al. In the $\delta + \gamma$ phase, they were quite different in the δ and γ phases. $D^{\delta+\gamma}$ was calculated by:^{27,28}

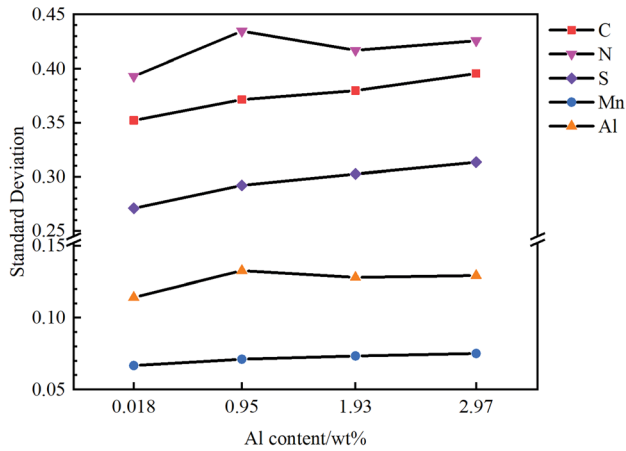


Fig. 8. The standard deviations of solutes C, N, S, Mn, and Al.

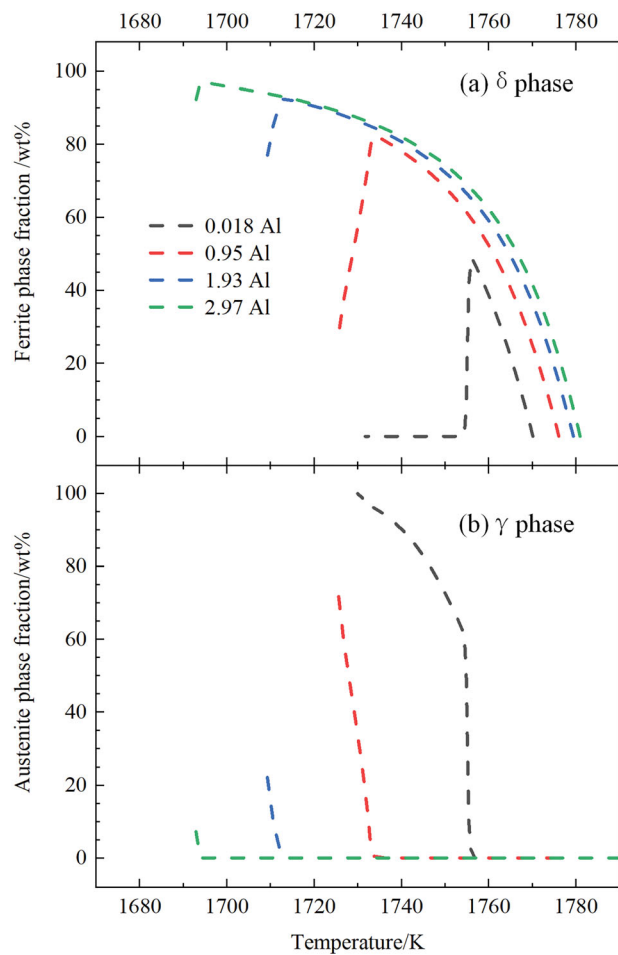


Fig. 9. The δ and γ phase fractions: (a) δ phase fraction; (b) γ phase fraction.

$$D^{\delta+\gamma} = V_{\delta} \cdot D^{\delta} + V_{\gamma} \cdot D^{\gamma} \quad (20)$$

$$V_{\delta} + V_{\gamma} = 1 \quad (21)$$

where D^{δ} , D^{γ} , and $D^{\delta+\gamma}$ are the diffusion coefficients in the δ , γ , and $\delta + \gamma$ phases, respectively, and V_{δ} and V_{γ} are the volume fractions of δ and γ in the solid phase, respectively. In the γ phase, the Al content has a slight influence on solutes Mn, S, C, and Al; however, the Al content has a great effect on solute N. In addition, the diffusion coefficients of solutes Mn, S, N, C, and Al in the γ phase were all smaller than those in the δ phase under different Al contents.

The average values of the diffusion coefficients are shown in Fig. 10f. With the Al content increasing from 0.018% to 0.95%, the values of the diffusion coefficients of the solute elements all greatly increased. This is because these solute elements diffuse faster in the δ phase, and the percentage of the δ phase increases. With the further increase of Al (from 0.95% to 2.97%), those diffusion coefficient values have slightly increased, and, in this range of Al content, the average values of solutes Mn, Al, S, N, and C were approximately 1.57×10^{-11} , 2.86×10^{-11} , 2.26×10^{-10} , 3.37×10^{-9} , and $7.45 \times 10^{-9} \text{ m}^2 \text{ s}^{-1}$, respectively. The diffusion coefficients of the solute elements were influenced by the addition of Al, and the order of the influence was $\text{Mn} > \text{Al} > \text{C} > \text{S} > \text{N}$. Accordingly, under different Al contents, the variation of the solute diffusion coefficients should be considered, and then used in the Clyne–Kurz model. A previous study showed that there was a slight effect of the solute diffusion coefficient on microsegregation,³⁴ because the solute diffusion coefficient was much smaller than the solute partition coefficient and had a low order of magnitude as a whole.

Formation Mechanism of AlN and MnS Inclusions

When the actual concentration products, Q_{AlN} and Q_{MnS} (by Eqs. 10–16), reached the equilibrium concentration products, K_{AlN} and K_{MnS} (by Eqs. 6 and 7), respectively, the AlN and MnS were able to form during solidification. As shown in Fig. S-1a (refer to online supplementary material), with the Al content increasing from 0.95% to 2.97%, the f_s of AlN precipitation decreased from 0.960 to 0.563, showing a large decrease. The addition of Al also has some effect on the formation of MnS, and the MnS precipitated earlier during solidification, with the f_s decreasing from 0.983 to 0.958, as shown in supplementary Fig. S-1b. Additionally, when the Al content is 0.018%, the AlN cannot precipitate during the solidification process. However, the addition of Al to medium manganese steel not only reduces the specific weight but also increases the stacking fault energy, and the addition of Al into medium manganese steel is necessary. When the Al content is 0.95%, the values for f_s of AlN precipitation and MnS precipitation are smaller than the 1.93% and 2.97% Al steel. Also, with the Al content increasing from 0.95% to 1.93%, the values for f_s of

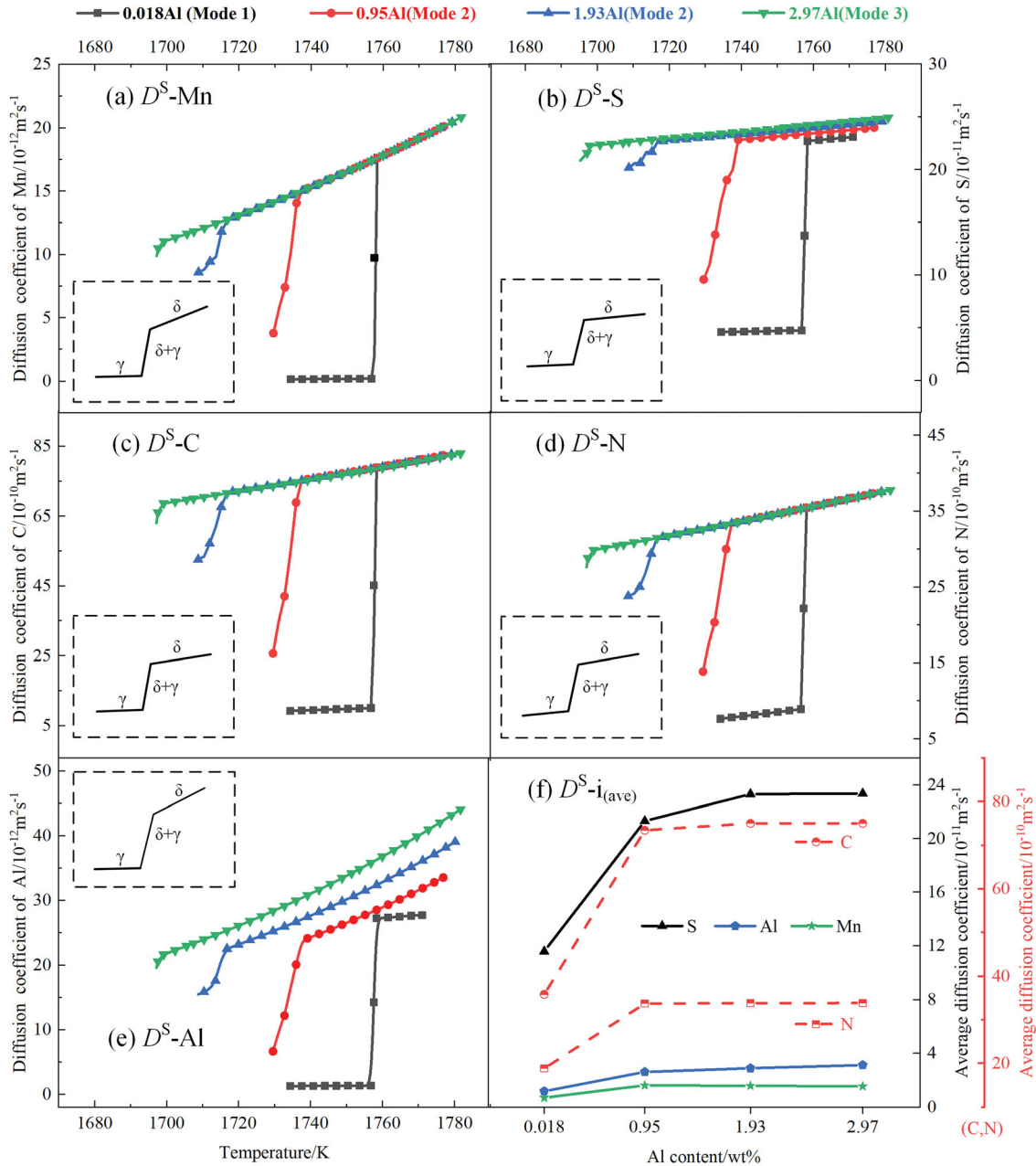


Fig. 10. The diffusion coefficients of solute elements in the solid phase calculated by DICTRA software: (a) D^S -Mn; (b) D^S -S; (c) D^S -C; (d) D^S -N; (e) D^S -Al; (f) D^S - $i_{(ave)}$.

AlN precipitation and MnS showed a large decrease. Therefore, in this study, the recommended range of Al content is 0.95% in medium manganese steel to control the precipitation of AlN and MnS inclusions.

The solid fraction has a relationship with the temperature,^{25,35} and the precipitation temperatures of AlN and MnS (T_{P-AlN} and T_{P-MnS}) can be obtained. The t_g (s) was the local growth time of AlN and MnS during solidification, defined as:³⁶

$$t_g = \frac{T_{P-AlN(MnS)} - T_S}{C_R} \quad (22)$$

where T_S is the solidus temperature from Table II, and the C_R is the cooling rate from Eq. 19.

As shown in supplementary Fig. S-2a, with the Al content increasing from 0.95% to 2.97%, the T_{P-AlN} increased from 1730 K to 1759 K, and the local growth time of AlN during solidification increased from 1.88 s to 26.6 s. For the AlN inclusions, the 2.97% Al steel possesses a higher local growth time, which provided a more sufficient condition for the growth of AlN. The addition of Al also has an effect on the formation of MnS, as shown in supplementary Fig. S-2b. With the Al content increasing from 0.018% to 2.97%, the T_{P-MnS} gradually decreased,

and the temperatures were 1732 K, 1729 K, 1717 K, and 1705 K, respectively. The local growth time of MnS during solidification increased from 0.80 s to 4.96 s, which showed a relative slight increase compared with the AlN inclusions.

CONCLUSION

The effect of Al content on the formation mechanism of AlN and MnS inclusions in Fe-5Mn-xAl-0.15C-0.23Si ($x = 0.018\%$, 0.95% , 1.93% , 2.97%) medium Mn steel was investigated by microstructure observation, thermodynamic analyses, and the Clyne–Kurz model. The effect of Al content on partition coefficient, diffusion coefficient, and secondary dendrite arm spacing was explored, and then these parameters under different Al contents were used in the Clyne–Kurz model. The main conclusions can be summarized as follows:

1. In Fe-5Mn-xAl-0.15C-0.23Si ($x = 0.018\%$, 0.95% , 1.93% , 2.97%) medium Mn steel, with the Al content increasing from 0.95% to 2.97% , the N contents of the formation of AlN decreased from 0.0151% to 0.0049% at the liquidus temperature. However, the critical N contents of the formation of AlN were still higher than the initial average content of N (0.0029%), so the AlN was unable to form in the liquid steel. With the Al content increasing from 0.018% to 2.97% , the S contents of the formation of MnS also decreased at the liquidus temperature, from 0.3960% to 0.3120% , which was much larger than the initial average content of S (0.0062%), and, therefore, the MnS cannot precipitate in the liquid steel.
2. The partition coefficients of the solute elements were easily influenced by the addition of Al during solidification, and the order of the influence was $S > C > N > Al > Mn$. With the Al content increasing from 0.018% to 2.97% , k_{Mn}^{ave} showed little change and was approximately 0.71 , k_N^{ave} first decreased from 0.47 to 0.30 ($0.018\text{--}0.95\%$) and then presented a slight increase to 0.33 (2.97%), and k_{Al}^{ave} showed the reverse trend with N. The values of k_S^{ave} and k_C^{ave} decreased continuously with the increase of Al from 0.018% to 2.97% , and the partition coefficients of S showed a large downward trend (from 0.0107 to 0.0060).
3. Based on EPMA, under the different Al contents, the concentrations of the solutes C, N, S, and Mn in the interdendritic area were higher than those in the dendrite zone, while the concentration distribution of solute Al was the opposite. The partition coefficients of solutes S, C, N, and Mn were all lower than 1, presenting positive segregation, while solute Al was higher than 1, showing negative segregation, which was consistent with the results by Thermo-Calc calculations.
4. The diffusion coefficients of the solute elements were influenced by the Al contents, and the order of the influence was $Mn > Al > C > S > N$. With the Al content increasing from 0.018% to 0.95% , the average values for the diffusion coefficients of the solute elements all greatly increased. This is because these elements diffuse faster in the δ phase, and so the percentage of the δ phase increases. With the further increase of Al (from 0.95% to 2.97%), those diffusion coefficient values slightly increased.
5. Based on the Clyne–Kurz model, with the Al content increasing from 0.95% to 2.97% , the precipitation temperature of AlN increased from 1730 K to 1759 K, and the local growth time of AlN during solidification increased from 1.88 s to 26.6 s. For AlN inclusions, the 2.97% Al steel possessed a higher local growth time, which provided a more sufficient condition for the growth of AlN. The local growth time of MnS increased from 0.80 s to 4.96 s, which showed a relatively slight increase compared with the AlN inclusions.

SUPPLEMENTARY INFORMATION

The online version contains supplementary material available at <https://doi.org/10.1007/s11837-024-06634-y>.

ACKNOWLEDGEMENTS

This work was supported by the National Natural Science Foundation of China (Nos. 51974079 and 52174310). The authors greatly appreciate their supports.

DATA AVAILABILITY

The raw and processed data required to reproduce these findings cannot be shared at this time as the data also forms part of an ongoing study.

CONFLICT OF INTEREST

The authors declare that they have no conflict of interest in this work.

REFERENCES

1. C.B. Finfrock, D. Bhattacharya, B.L. McBride, T.J. Ballard, A.J. Clarke, and K.D. Clarke, *JOM* 74, 506 (2022).
2. S. Li, S. Yang, Y. Lu, H. Luo, and W. Tao, *Metall. Trans. B* 50, 1 (2019).
3. Y. Wang, S. Zhao, R. Song, and B. Hu, *Int. J. Miner. Metall. Mater.* 28, 422 (2021).
4. C.-Y. Lee and Y.-K. Lee, *JOM* 66, 1794 (2014).
5. H. Zhang, M. Cai, W. Zhu, S. Sun, H. Yan, S. Yao, Y. Luan, S. Tang, and P.D. Hodgson, *Metall. Trans. A* 53, 3869 (2022).
6. H. Chen, H. Xu, T. Zhou, and Z. Chen, *JOM* 74, 2826 (2022).

7. H.H. Dickert, P. Suwanpinij, and W. Bleck, *Steel Res. Int.* 93, 2100622 (2022).
8. X. Xin, J. Yang, Y. Wang, R. Wang, W. Wang, H. Zheng, and H. Hu, *Ironmak. Steelmak.* 43, 234 (2016).
9. J. Chu, L. Zhang, J. Yang, Y. Bao, N. Ali, and C. Zhang, *Mater. Charac.* 194, 112367 (2022).
10. W. Wang, T. Luo, Z. Liu, S. Luo, and M. Zhu, *Metall. Trans. B* 54, 274 (2023).
11. Q. Tian, G. Wang, Y. Zhao, J. Li, and Q. Wang, *Metall. Trans. B* 49, 1149 (2018).
12. T.F. Bower, H. Brody, and M.C. Flemings, *Metall. Soc. AIME* 236, 624 (1966).
13. T.W. Clyne and W. Kurz, *Metall. Trans. A* 12, 965 (1981).
14. D. You, S.K. Michelic, C. Bernhard, D. Loder, and G. Wieser, *ISIJ Int.* 56, 1770 (2016).
15. V.R. Voller and C. Beckermann, *Metall. Trans. A* 30, 2183 (1999).
16. Y. Guo, L. Cao, G. Wang, and C. Liu, *Metall. Trans. B* 54, 275 (2023).
17. T. Zhang, Y. Chen, G. Cheng, X. Yang, X. Chen, J. Pan, Y. Huang, and Q. Wang, *Steel Res. Int.* 93, 2200478 (2022).
18. L. Jin, S. Zheng, and M. Zhu, *JOM* 75, 2235 (2023).
19. M. Nabeel, M. Alba, A. Karasev, P.G. Jönsson, and N. Dogan, *Metall. Trans. B* 50, 1674 (2019).
20. M. Alba, M. Nabeel, and N. Dogan, *Steel Res. Int.* 91, 1900477 (2020).
21. D. Liu, Z. Xue, and S. Song, *Steel Res. Int.* 93, 2200551 (2022).
22. H. Liu, J. Liu, S.K. Michelic, S. Shen, X. Su, B. Wu, and H. Ding, *Steel Res. Int.* 87, 1723 (2016).
23. S.K. Choudhary, and A. Ghosh, *ISIJ Int.* 49, 1819 (2021).
24. P. Lu, H. Li, H. Feng, Z. Jiang, H. Zhu, Z. Liu, and T. He, *Metall. Trans. B* 52, 2210 (2021).
25. Y. Liu, L. Zhang, H. Duan, Y. Zhang, Y. Luo, and A.N. Conejo, *Metall. Trans. A* 47, 3015 (2016).
26. J. Liu, C. Liu, R. Bai, W. Wang, Q. Wang, H. Zhang, and H. Ni, *Metall. Trans. B* 54, 685 (2023).
27. Y. Huang, M. Long, P. Liu, D. Chen, H. Chen, L. Gui, T. Liu, and S. Yu, *Metall. Trans. B* 48, 2504 (2017).
28. Y. Ueshima, S. Mizoguchi, T. Matsumiya, and H. Kajioka, *Metall. Trans. B* 17, 845 (1986).
29. Y.-M. Won and B.G. Thomas, *Metall. Trans. A* 32, 1755 (2001).
30. Y. Shen, S. Yang, J. Liu, H. Liu, R. Zhang, H. Xu, and Y. He, *Steel Res. Int.* 90, 1800546 (2019).
31. Y. Shen, J. Liu, H. Xu, and H. Liu, *Metall. Trans. B* 51, 2963 (2020).
32. J. Yoo, B. Kim, Y. Park, and C. Lee, *J. Mater. Sci.* 50, 279 (2015).
33. H. Liu, J. Liu, B. Wu, Y. Shen, Y. He, H. Ding, and X. Su, *Mater. Sci. Eng. A* 708, 360 (2017).
34. L. Gui, M. Long, Y. Huang, D. Chen, H. Chen, H. Duan, and S. Yu, *Metall. Trans. B* 49, 3280 (2018).
35. Y. Wang, J. Yang, X. Xin, R. Wang, and L. Xu, *Metall. Trans. B* 47, 1378 (2016).
36. Z. Xue, N. Li, L. Wang, S. Song, D. Liu, and A. Huang, *Metall. Trans. B* 52, 3860 (2021).

Publisher's Note Springer Nature remains neutral with regard to jurisdictional claims in published maps and institutional affiliations.

Springer Nature or its licensor (e.g. a society or other partner) holds exclusive rights to this article under a publishing agreement with the author(s) or other rightsholder(s); author self-archiving of the accepted manuscript version of this article is solely governed by the terms of such publishing agreement and applicable law.